XII International Conference on Computational Plasticity. Fundamentals and Applications
COMPLAS XII
E. Oñate, D.R.J. Owen, D. Peric and B. Suárez (Eds)

HOMOGENIZATION OF HETEROGENEOUS, FIBRE STRUCTURED MATERIALS

S. FILLEP*, J. MERGHEIM* AND P. STEINMANN*

* Chair of Applied Mechanics
University Erlangen-Nuremberg
Egerlandstr. 5, 91058 Erlangen, Germany
e-mail: {sebastian.fillep, julia.mergheim, paul.steinmann}@ltm.uni-erlangen.de

Key words: Homogenization, Hysteresis, Contact, Technical Textiles, Multi-Scale, Shell Kinematic.

Abstract. This contribution presents a multi-scale homogenization method to model fibre structured materials. On the macroscopic level textiles are characterized by a large area-to-thickness ratio, such that a discretization with shell elements is numerically efficient. The material behavior is strongly influenced by the heterogeneous micro structure. To capture the contact on the micro level, the RVE is explicitly modelled by means of a volumetric micro sample and a shell specific homogenization scheme is applied to transfer the microscopic response to the macro level. Theoretical aspects are discussed and a numerical example for contact behavior of a periodic knitted structure is given.

1 INTRODUCTION

The consideration of material behavior at different length scales is essential to understand the behavior of heterogeneous materials and define adequate constitutive laws. Using suitable homogenization techniques permits to develop reliable scale transitions between the connected levels [1]. The challenge is to transfer the information across length scales. Within homogenization based approaches the macroscopic constitutive behavior of the inhomogeneous material is modelled by means of an appropriate micro scale representative volume element (RVE). For each macro scale material point a fine scale boundary value problem is solved to determine the local material behavior on the large scale. For nonlinear material behavior the FE^2 method is often applied which involves the simultaneous solution of the macro and the micro scale problems within a nested solution scheme [2, 4]. However, it is also possible to systematically create data for macroscopic stress-strain states by applying a range of deformations to the RVE and evaluating the homogenized stress response [5].

The macroscopic material behavior of textiles is usually nonlinear and depends strongly on the heterogeneities on the micro level, i.e. on the structural assembly of the fibres. The

macroscopic nonlinear material characteristic results mainly from the contact interaction between the fibres.

The macroscopic technical textile can be considered as a shell structure, which is numerically efficient [7, 6]. To capture the microscopic behavior a volumetric RVE is defined [8, 9] that explicitly models the fibres and the contact interaction between them.

In this paper a homogenization procedure is introduced that combines a macroscopic shell with a microscopic volumetric RVE. Therefore a homogenization scheme is derived, which connects the macro scale to the micro scale problem. For the representation of the micro level a suitable micro sample is defined and the macroscopic behavior is derived by homogenization of the micro structural response. Finally a numerical example is given to test the derived homogenization scheme and characterize the resulting hysteretic behavior due to the contact.

2 THE REPRESENTATIVE VOLUME ELEMENT

Homogenization schemes are usually based on the assumption that the considered length scales are well separated, i.e. the microscopic length scale l_m is much smaller than the macroscopic one $l_m \ll l$. This assumption is violated when the micro structural size is no longer negligible with respect to the macro structural size. This situation occurs when shells are considered. Here, the separation of length scales is only given in plane direction. Microscopic and macroscopic thickness are the same. To take this into account a shell specific homogenization scheme is introduced that uses the quasi second order assumptions for a shell continuum.

In this context the principle of separation of length scales becomes relaxed for the thickness direction, where macroscopic and microscopic length are considered the same

$$H_m = H \ . \tag{1}$$

The considered textile consists of a periodic assembly of fibres, as shown in figure 1. The

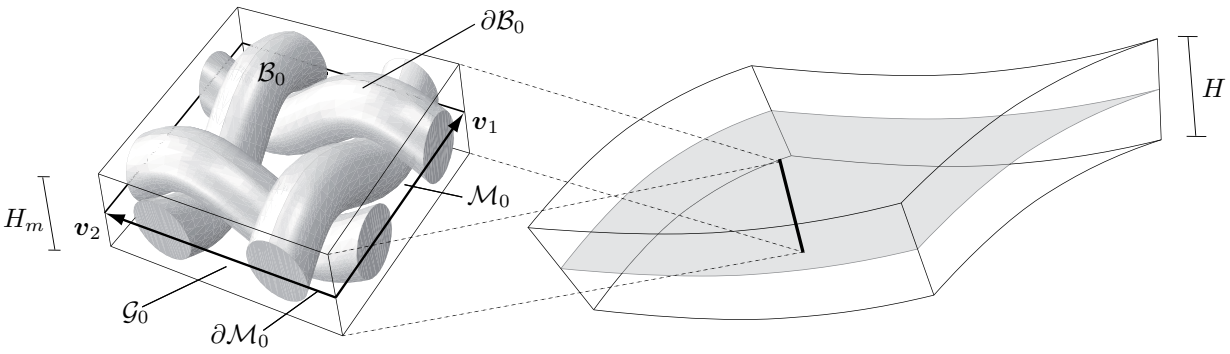

Figure 1: Determination of an unit cell

minimal sample that can be used as a representative volume element is the unit cell.

The unit cell is spanned by a periodicity frame. The periodicity frame is characterized by two independent vectors $\boldsymbol{v}_1$ and $\boldsymbol{v}_2$ having the property that the mechanical characteristics are invariant along any translation $m_1\boldsymbol{v}_1 + m_2\boldsymbol{v}_2$, where m_1 and m_2 are integer numbers. The RVE of the textile consists of different parts, a material volume part $\mathcal{B}_0$ and a material free part $\mathcal{G}_0$ such that $\mathcal{V}_0 = \mathcal{B}_0 \cup \mathcal{G}_0$ is the RVE volume. Normal to the thickness direction the mid-surface $\mathcal{M}_0$ is defined.

3 MACROSCOPIC SHELL KINEMATICS

A body $\mathcal{B}$ is a collection of material points $\mathcal{P}$ with $\boldsymbol{X}$ denoting the position of $\mathcal{P}$ in the material configuration $\mathcal{B}_0$ at time t_0 in the three dimensional Euclidean vector space $\mathbb{E}^3$. The nonlinear deformation map to the current configuration $\mathcal{B}_t$ is defined by

$$\boldsymbol{\varphi}(\boldsymbol{X}, t) = \boldsymbol{x} \ , \tag{2}$$

where $\boldsymbol{x}$ indicates the position of the material point $\mathcal{P}$ at the time t_t.

The geometry and deformation of a shell is described by curvilinear convective coordinates θ^i as given in figure 3. The position is typically specified via the shell middle surface $\mathcal{M}_0$ where $\theta^3 = 0$. In the further course Latin indices range from 1 to 3 and Greek indices range from 1 to 2. The position and deformation map of a finite deformation shell are specified as

$$\boldsymbol{X}(\theta^i) = \widehat{\boldsymbol{X}}(\theta^\alpha) + \theta^3 \boldsymbol{D}(\theta^\alpha) \quad \text{and} \quad \boldsymbol{\varphi}(\theta^i) = \widehat{\boldsymbol{\varphi}}(\theta^\alpha) + \theta^3 \boldsymbol{d}(\theta^\alpha) \ . \tag{3}$$

The vectors $\widehat{\boldsymbol{X}}$ and $\widehat{\boldsymbol{\varphi}}$ provide a parametric representation of the middle surface of the shell in the reference and the current state. The parameter $\theta^3 = [-\frac{1}{2}, \frac{1}{2}]$ determines the position of a point normal to the middle surface in the undeformed state. Furthermore, $||\boldsymbol{D}|| = H_0$ and $||\boldsymbol{d}|| = H_t$ are the absolute values of the shell thickness. The thickness stretch is denoted by $\lambda_3 = \frac{H_t}{H_0}$, which means that the displacement in thickness direction is approximated linearly. A result of this approximation is the distortion freedom of the shell cross section. The displacement can be calculated by the difference of the spatial and material position

$$\boldsymbol{u}(\theta^i) = \widehat{\boldsymbol{\varphi}}(\theta^\alpha) - \widehat{\boldsymbol{X}}(\theta^\alpha) + \theta^3[\boldsymbol{d} - \boldsymbol{D}] \ . \tag{4}$$

All kinematic values can be calculated, if the shell geometry in the material and the spatial configuration are known. The covariant basis vectors on the middle surface of the shell can then be developed from the partial derivative of the material vector $\widehat{\boldsymbol{X}}$ and the spatial vector $\widehat{\boldsymbol{\varphi}}$ with respect to the curvilinear coordinates

$$\boldsymbol{A}_\alpha = \frac{\partial \widehat{\boldsymbol{X}}}{\partial \theta^\alpha} = \widehat{\boldsymbol{X}}_{,\alpha} \ , \quad \boldsymbol{A}_3 = \boldsymbol{X}_{,3} = \boldsymbol{D} \ , \quad \boldsymbol{a}_\alpha = \frac{\partial \widehat{\boldsymbol{\varphi}}}{\partial \theta^\alpha} = \widehat{\boldsymbol{\varphi}}_{,\alpha} \ , \quad \boldsymbol{a}_3 = \boldsymbol{d} \ . \tag{5}$$

For the macro to micro scale transition the shell formulation has to be extended to a three

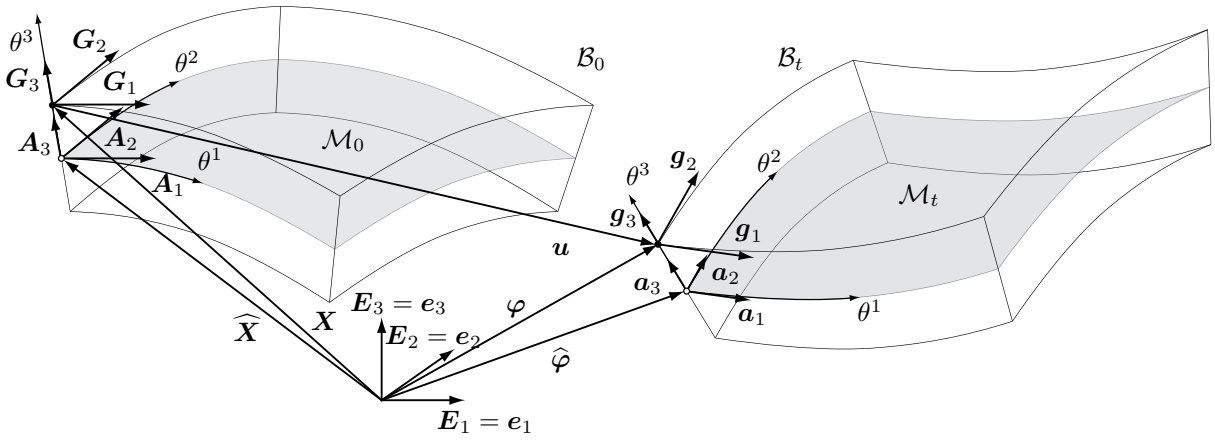

Figure 2: Shell kinematics

dimensional formulation. From equation (3) covariant basis vectors for the description of the shell body can be derived as

$$\boldsymbol{G}_i = \frac{\partial \boldsymbol{X}}{\partial \theta^i} \qquad \text{and} \qquad \boldsymbol{g}_i = \frac{\partial \boldsymbol{x}}{\partial \theta^i} \,, \tag{6}$$

and specified by introducing equations (3) and (5) as

$$\begin{aligned} \boldsymbol{G}_\alpha &= \frac{\partial \boldsymbol{X}}{\partial \theta^\alpha} = \frac{\partial \widehat{\boldsymbol{X}}}{\partial \theta^\alpha} + \theta^3 \frac{\partial \boldsymbol{D}}{\partial \theta^\alpha} = \boldsymbol{A}_\alpha + \theta^3 \boldsymbol{A}_{3,\alpha} \,, \quad \boldsymbol{G}_3 = \frac{\partial \boldsymbol{X}}{\partial \theta^3} = \boldsymbol{A}_3 \,, \\ \boldsymbol{g}_\alpha &= \frac{\partial \boldsymbol{\varphi}}{\partial \theta^\alpha} = \frac{\partial \widehat{\boldsymbol{\varphi}}}{\partial \theta^\alpha} + \theta^3 \frac{\partial \boldsymbol{d}}{\partial \theta^\alpha} = \boldsymbol{a}_\alpha + \theta^3 \boldsymbol{a}_{3,\alpha} \,, \quad \boldsymbol{g}_3 = \frac{\partial \boldsymbol{\varphi}}{\partial \theta^3} = \boldsymbol{a}_3 \,. \end{aligned} \tag{7}$$

The contravariant basis vectors result from the relations

$$\boldsymbol{G}^i \cdot \boldsymbol{G}_j = \delta^i_j \qquad \text{and} \qquad \boldsymbol{g}^i \cdot \boldsymbol{g}_j = \delta^i_j \,, \tag{8}$$

with the Kronecker delta δ^i_j. The covariant vectors are tangents to the coordinate lines and the contravariant vectors are normal to the coordinate surfaces. The deformation gradient $\boldsymbol{F}$ is defined to be the spatial derivative of $\boldsymbol{\varphi}$

$$\boldsymbol{F} = \frac{\partial \boldsymbol{\varphi}}{\partial \boldsymbol{X}} = \frac{\partial \boldsymbol{\varphi}}{\partial \theta^i} \otimes \frac{\partial \theta^i}{\partial \boldsymbol{X}} = \boldsymbol{g}_i \otimes \boldsymbol{G}^i \,, \tag{9}$$

and with equation (7) results in

$$\boldsymbol{F} = [\boldsymbol{a}_\alpha + \theta^3 \boldsymbol{a}_{3,\alpha}] \otimes \boldsymbol{G}^\alpha + \boldsymbol{a}_3 \otimes \boldsymbol{G}^3 \,. \tag{10}$$

The variation of $\boldsymbol{F}$ reads

$$\delta \boldsymbol{F} = [\delta \boldsymbol{a}_\alpha + \theta^3 \delta \boldsymbol{a}_{3,\alpha}] \otimes \boldsymbol{G}^\alpha + \delta \boldsymbol{a}_3 \otimes \boldsymbol{G}^3 \,. \tag{11}$$

Finally, the internal power of a shell can be specified in work conjugate quantities i.e. the Piola-Kirchhoff stress $\boldsymbol{P}$ and the variation of the deformation gradient $\boldsymbol{F}$ as

$$\begin{aligned}
\mathcal{U}^{INT} &= \int_{\mathcal{B}_0} \boldsymbol{P} : \delta\boldsymbol{F} dV = \iiint \sqrt{G}\, \boldsymbol{P} : \delta\boldsymbol{F} d\theta^3 d\theta^2 d\theta^1 \\
&= \iiint \sqrt{G}\, [\delta\boldsymbol{a}_\alpha \cdot \boldsymbol{P} \cdot \boldsymbol{G}^\alpha + \theta^3 \delta\boldsymbol{d}_{,\alpha} \cdot \boldsymbol{P} \cdot \boldsymbol{G}^\alpha + \delta\boldsymbol{d} \cdot \boldsymbol{P} \cdot \boldsymbol{G}^3] d\theta^3 d\theta^2 d\theta^1 \\
&= \iint \delta\boldsymbol{a}_\alpha \cdot \int \underbrace{\sqrt{G}\, \boldsymbol{P} \cdot \boldsymbol{G}^\alpha}_{\boldsymbol{t}_0^\alpha} d\theta^3 d\theta^2 d\theta^1 + \iint \delta\boldsymbol{d}_{,\alpha} \cdot \int \theta^3 \underbrace{\sqrt{G}\, \boldsymbol{P} \cdot \boldsymbol{G}^\alpha}_{\boldsymbol{t}_0^\alpha} d\theta^3 \boldsymbol{m}^\alpha d\theta^2 d\theta^1 \\
&\quad + \iint \delta\boldsymbol{d} \cdot \int \underbrace{\sqrt{G}\, \boldsymbol{P} \cdot \boldsymbol{G}^3}_{\boldsymbol{t}_0^3} d\theta^3 \boldsymbol{n}^3 d\theta^2 d\theta^1 = \iint [\delta\boldsymbol{a}_\alpha \cdot \boldsymbol{n}^\alpha + \delta\boldsymbol{d}_{,\alpha} \cdot \boldsymbol{m}^\alpha + \delta\boldsymbol{d} \cdot \boldsymbol{n}^3] d\theta^2 d\theta^1 \ ,
\end{aligned} \tag{12}$$

where a volume element dV of the reference volume $\mathcal{B}_0$ is defined as $dV = \sqrt{G} d\theta^1 d\theta^2 d\theta^3$ with $\sqrt{G} = [\boldsymbol{G}_1 \times \boldsymbol{G}_2] \cdot \boldsymbol{G}_3$.The volume integral is separated into the integral over the middle surface $\mathcal{M}_0$ and a through thickness integration. Then the variation of the deformation gradient (11) is introduced and the multiplication of $\boldsymbol{P}$ with the contravariant basis vectors yields tractions $\boldsymbol{t}_0^i$, which are subsequently transformed to stress resultants $\boldsymbol{n}^i$ and $\boldsymbol{m}^\alpha$ by a pre-integration in thickness direction. In the particular case of resulting moments the tractions are multiplied with the lever arm θ^3. These stress resultants exist with respect to the middle surface.

4 HOMOGENIZATION FOR SHELLS

A basic concept of scale transition is the equality of the averaged macroscopic and the microscopic internal power density. For the homogenization scheme a power averaging theorem is introduced, which is a special format of the known Hill-Mandel condition. The macroscopic internal power density has to be equal to the microscopic internal power density averaged over the middle surface $\mathcal{M}_0$ of the RVE

$$\wp^{INT} = \frac{1}{A_{0,m}} \int_{\mathcal{B}_{0,m}} \wp_m^{INT} dV \ , \tag{13}$$

where $A_{0,m}$ is the measure of the middle surface in the parameter space of θ^1, θ^2. A characteristic of the shell specific homogenization scheme is that the microscopic representative volume element is related to a straight line normal to the middle surface through the thickness of the shell as depicted in figure 1. This is a result from the shell assumption and the pre-integration over the thickness of the RVE to transfer all quantities to the middle surface. The Hill-Mandel condition can be recast in a formulation with work

conjugated quantities like the deformation gradient and the Piola-Kirchhoff stress

$$\delta \boldsymbol{a}_\alpha \cdot \boldsymbol{n}^\alpha + \delta \boldsymbol{d}_{,\alpha} \cdot \boldsymbol{m}^\alpha + \delta \boldsymbol{d} \cdot \boldsymbol{n}^3 = \frac{1}{A_{0,m}} \int\limits_{\mathcal{B}_{0,m}} \boldsymbol{P}_m : \delta \boldsymbol{F}_m dV \ . \tag{14}$$

The macroscopic deformation gradient is assumed to be equal to the microscopic averaged deformation gradient

$$\begin{aligned} \boldsymbol{F} &= \frac{1}{V_{0,m}} \int\limits_{\mathcal{B}_{0,m}} \boldsymbol{F}_m dV = \frac{1}{A_{0,m}} \iint \sqrt{G} \left[\frac{1}{H_0} \int \boldsymbol{F}_m d\theta^3 \right] d\theta^2 d\theta^1 \\ &= \frac{1}{A_{0,m}} \iint \frac{\sqrt{G}}{H_0} \left[\boldsymbol{a}^m_\alpha \otimes \int \boldsymbol{G}^\alpha_m d\theta^3 + \boldsymbol{d}^m_{,\alpha} \otimes \int \theta^3 \boldsymbol{G}^\alpha_m d\theta^3 + \boldsymbol{d}^m \otimes \int \boldsymbol{G}^3_m d\theta^3 \right] d\theta^2 d\theta^1 \ , \end{aligned} \tag{15}$$

The macroscopic and the microscopic covariant basis vectors in the reference state are assumed to be equal, $\boldsymbol{G}^i = \boldsymbol{G}^i_m$, as the initial, internal curvature of the RVE is negligible. The position of a microscopic material point in the spatial configuration $\boldsymbol{\varphi}_m$ on the micro scale is given by

$$\boldsymbol{\varphi}_m = \boldsymbol{F} \cdot \boldsymbol{X}_m + \boldsymbol{w} \ , \tag{16}$$

where $\boldsymbol{X}_m$ is the position of the microscopic material point in the material configuration and $\boldsymbol{w}$ is the microscopic fluctuation field. By applying the gradient with respect to the current position ∇_X the microscopic deformation gradient $\boldsymbol{F}_m$ is given by

$$\boldsymbol{F}_m = \boldsymbol{F} + \nabla_X \boldsymbol{w} \ . \tag{17}$$

The fluctuation field $\boldsymbol{w}$ is expressed in a shell specific formulation according to (3) as

$$\boldsymbol{w} = \widehat{\boldsymbol{w}}(\theta^\alpha_m) + \theta^3 \boldsymbol{d}^w(\theta^\alpha_m) \ , \tag{18}$$

with the part in shell plane direction $\widehat{\boldsymbol{w}}(\theta^\alpha)$ and the fluctuation of the director $\boldsymbol{d}^w(\theta^\alpha)$. The gradient of the fluctuation results as

$$\nabla_X \boldsymbol{w} = [\widehat{\boldsymbol{w}}_{,\alpha} + \theta^3 \boldsymbol{d}^w_{,\alpha}] \otimes \boldsymbol{G}^\alpha + \boldsymbol{d}^w \otimes \boldsymbol{G}^3 \ . \tag{19}$$

The covariant basis vectors in the spatial configuration on the middle surface are defined as

$$\boldsymbol{a}^w_\alpha = \frac{\partial \widehat{\boldsymbol{w}}}{\partial \theta^\alpha} = \widehat{\boldsymbol{w}}_{,\alpha} \quad , \quad \boldsymbol{a}^w_3 = \boldsymbol{d}^w \ . \tag{20}$$

These can be extended to a three dimensional formulation

$$\boldsymbol{g}^w_\alpha = \frac{\partial \boldsymbol{w}}{\partial \theta^\alpha} = \widehat{\boldsymbol{w}}_{,\alpha} + \theta^3 \boldsymbol{d}^w_{,\alpha} \quad , \quad \boldsymbol{g}^w_3 = \boldsymbol{d}^w \ . \tag{21}$$

By introducing the microscopic kinematic relations into the Hill-Mandel condition (14), it can be written as

$$\begin{aligned}
&\delta \boldsymbol{a}_\alpha \cdot \boldsymbol{n}^\alpha + \delta \boldsymbol{d}_{,\alpha} \cdot \boldsymbol{m}^\alpha + \delta \boldsymbol{d} \cdot \boldsymbol{n}^3 \\
&\doteq \frac{1}{A_{0,m}} \left[\iint \delta \boldsymbol{a}_\alpha \cdot \boldsymbol{n}_m^\alpha d\theta^2 d\theta^1 + \iint \delta \boldsymbol{d}_{,\alpha} \cdot \boldsymbol{m}_m^\alpha d\theta^2 d\theta^1 + \iint \delta \boldsymbol{d} \cdot \boldsymbol{n}_m^3 d\theta^2 d\theta^1 \right] \\
&\quad + \frac{1}{A_{0,m}} \iint [\delta \widehat{\boldsymbol{w}}_{,\alpha} \cdot \boldsymbol{n}_m^\alpha + \delta \boldsymbol{d}_{,\alpha}^w \cdot \boldsymbol{m}_m^\alpha + \delta \boldsymbol{d}^w \cdot \boldsymbol{n}_m^3] d\theta^2 d\theta^1
\end{aligned} \tag{22}$$

and the following macroscopic quantities (or stress resultants) can be identified

$$\begin{aligned}
\boldsymbol{n}^\alpha &= \frac{1}{A_{0,m}} \iint \boldsymbol{n}_m^\alpha d\theta^2 d\theta^1 \quad \text{with} \quad \boldsymbol{n}_m^\alpha = \int \sqrt{G}\, \boldsymbol{P}_m \cdot \boldsymbol{G}^\alpha d\theta^3 = \int \boldsymbol{t}_{0,m}^\alpha d\theta^3 \,, \\
\boldsymbol{m}^\alpha &= \frac{1}{A_{0,m}} \iint \boldsymbol{m}_m^\alpha d\theta^2 d\theta^1 \quad \text{with} \quad \boldsymbol{m}_m^\alpha = \int \sqrt{G}\, \theta^3 \boldsymbol{P}_m \cdot \boldsymbol{G}^\alpha d\theta^3 = \int \theta^3 \boldsymbol{t}_{0,m}^\alpha d\theta^3 \,, \\
\boldsymbol{n}^3 &= \frac{1}{A_{0,m}} \iint \boldsymbol{n}_m^3 d\theta^2 d\theta^1 \quad \text{with} \quad \boldsymbol{n}_m^3 = \int \sqrt{G}\, \boldsymbol{P}_m \cdot \boldsymbol{G}^3 d\theta^3 = \int \boldsymbol{t}_{0,m}^3 d\theta^3 \,.
\end{aligned} \tag{23}$$

Due to introduction of periodic boundary conditions with periodic fluctuations $\boldsymbol{w}^+ = \boldsymbol{w}^-$ and antiperiodic tractions $\boldsymbol{t}^+ = -\boldsymbol{t}^-$ on opposite sides of the mid-surface edge curves $\partial\mathcal{M}_0^+$ and $\partial\mathcal{M}_0^-$ of it follows that the part of the internal power related to the fluctuations averaged over the RVE disappears as shown in detail in [3].

5 COMPUTATIONAL EXAMPLES

In the second example a prismatic cutout of a knitted textile structure with the dimensions $6.8 \times 8.0 \times 4.2$ mm is determined as the representative micro sample. To represent the fibres ideal cylindrical monofilaments are assumed with a fibre diameter of 1.25 mm as depicted in figure 3. The microscopic mesh is composed of about 7100 elements with

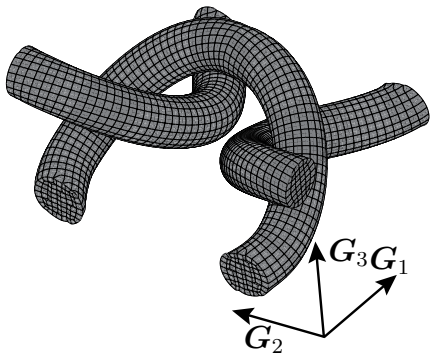

Figure 3: The discretized knitted representative volume element

quadratic interpolation. For this RVE a cyclic loading deformation is considered and the

macroscopic homogenized stresses are analyzed.For the sake of simplicity, the constitutive behavior of the fibres is modelled linear elastic, defined by the following constitutive equation

$$\boldsymbol{\sigma} = \frac{E}{1+\nu}\left[\frac{\nu}{1-2\nu} tr(\boldsymbol{\varepsilon})\boldsymbol{I} + \boldsymbol{\varepsilon}\right] , \tag{24}$$

where $\boldsymbol{\sigma}$ denotes the Cauchy stress, $\boldsymbol{\varepsilon}$ the linearized strain, $tr(\boldsymbol{\varepsilon})$ the trace of the strain tensor, E the Young's modulus and ν the Poisson's ratio. The material parameters used are characteristically for the elastic behavior of polymers, e.g., polyamide with $E = 2000$ N/mm^2 and $\nu = 0.33$.

The boundary of the material volume part of the RVE $\partial\mathcal{B}_0$ can be split in three non-overlapping parts $\partial\mathcal{B}_{0,N}$, $\partial\mathcal{B}_{0,D}$ and $\partial\mathcal{B}_{0,C}$ with $\partial\mathcal{B}_{0,N} \cup \partial\mathcal{B}_{0,D} \cup \partial\mathcal{B}_{0,C} = \partial\mathcal{B}_0$ and $\partial\mathcal{B}_{0,N} \cap \partial\mathcal{B}_{0,D} \cap \partial\mathcal{B}_{0,C} = \emptyset$. The body is submitted to a Neumann condition on $\partial\mathcal{B}_{0,N}$, to a Dirichlet condition on $\mathcal{B}_{0,D}$ and an unilateral contact condition with Coulomb law of friction

$$|\boldsymbol{t}_t| = \mu\, t_n \text{ with } \quad t_n \geq 0 , \tag{25}$$

between the fibre bodies on $\partial\mathcal{B}_{0,C}$, where $\boldsymbol{t}_t$ are the tangential tractions and t_n are the tractions normal to the contact surface. The normal contact condition is exactly enforced by the Lagrange multiplier method in contrast to the tangential contact, which is treated by a Penalty method. For the relation of the normal and the tangential tractions a friction coefficient is introduced and no distinction is made between the static and the slip friction coefficient $\mu_0 = \mu$. The Neumann boundary is composed by the top and bottom faces of the micro shell element, where zero traction conditions are applied. This condition is relevant for shells that are not loaded in the out of plane direction and leaves the thickness strain undetermined, which is accordingly a result from the micro calculation. The other two pairs of boundary surfaces are the Dirichlet boundary, where the former introduced periodic boundary conditions are applied that transfer the macroscopic deformation to the micro level. Through the periodicity conditions the freedom of distortion of the shell cross sections is relaxed. The considered knitted textile is now loaded in $\boldsymbol{G}_1$ direction

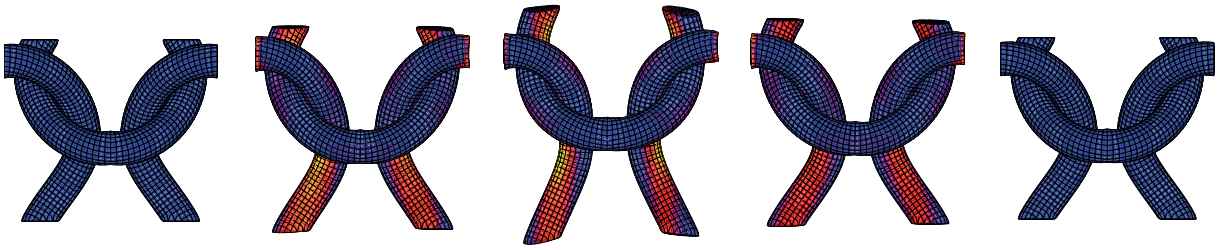

Figure 4: Plot of the von Mises stress on the current state of the cyclic loaded knitted RVE for 0, 25, 50, 75 and 100 % of the cycle time.

by a tensile loading. The entry of the macroscopic deformation gradient is increased to a maximum value of $\varphi_1^1 = 1.3$. Thereafter the loading is relaxed to the reference

state value. the other deformation modes and curvatures are set to zero. The stretch in thickness direction stays undetermined, consequently the plane stress assumption holds.

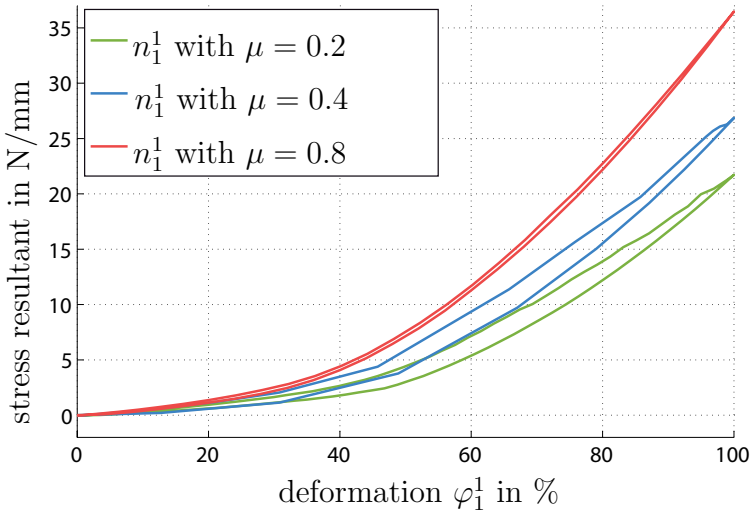

Figure 5: Plot of the normal force n_1^1 over the cyclic deformation for different friction coefficients.

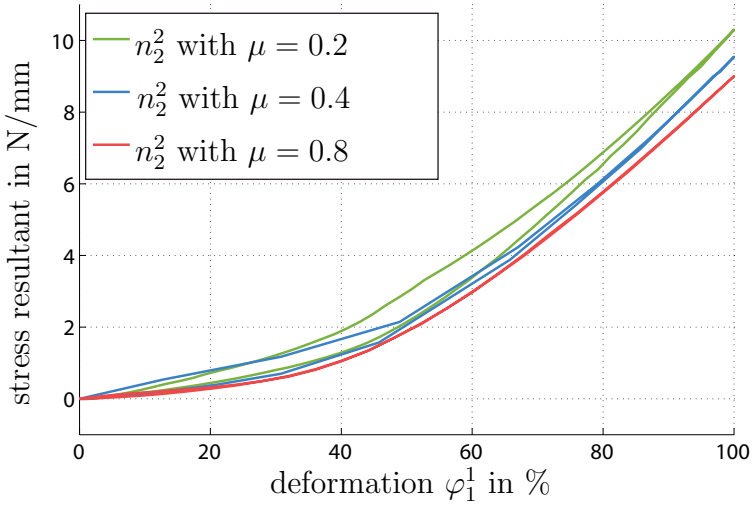

Figure 6: Plot of the normal force n_2^2 over the cyclic deformation for different friction coefficients.

Therewith a parameter study of the friction coefficient μ is performed. In figure 4 plots of the von Mises stress on the current state of the cyclic loaded knitted RVE for for different states of the cycle time are depicted. In figure 5 the hysteretic behavior of a single loading cycle is depicted by capturing the stress-resultant n_1^1 in $\boldsymbol{G}_1$ direction over the normalized deformation. Although the fibre material is modelled linear elastically, the structure

shows a nonlinear progressive constitutive behavior. During the cycle irreversible slip occurs which is indicated by the hysteretic behavior. The overall stiffness of the structure increases with the increase of the friction coefficient.

In figure 6 the normal stress resultant in $\boldsymbol{G}_2$ direction is depicted, which results from the restricted transversal contraction. A hysteretic behavior can be observed as well. The stiffness in $\boldsymbol{G}_2$ direction increases with decreasing friction coefficient, which results from the structural assembly of the fibres.

6 CONCLUSIONS

In this work a multi-scale homogenization approach for technical textiles has been introduced. The scale transition between a macroscopic shell and a microscopic three dimensional heterogeneous structure is developed. On the micro scale contact interaction between fibres is taken into account that causes nonlinear constitutive behavior. Main focus was put on the development of the work conjugate quantities like shell specific deformations and stress resultants. A special format of the Hill-Mandel condition was developed that allows to derive appropriate boundary conditions for the RVE. An analysis of the homogenized stress resultants friction coefficients was shown.

REFERENCES

[1] C. Miehe, *Computational micro-to-macro transitions for discretized micro-structures of heterogeneous materials at finite strains based on the minimization of averaged incremental energy*, Comput. Methods in App. Mech. Eng., **192**, pp. 559-591, (2003)

[2] V.G. Kouznetsova, M.G.D Geers, W.A.M. Brekelmans, *Multi-scale second-order computational homogenization of multi-phase materials: a nested finite element solution strategy*, Comput. Methods in App. Mech. Eng., **193**, pp. 5525-5550 , (2004)

[3] S. Fillep, J. Mergheim, P. Steinmann, *Computational meodelling and homogenization of technical textiles*, Engineering Structures, **50**, pp. 68-73, (2013)

[4] P. Ponte Castañeda , E. Tiberio, *A second-order homogenization method in finite elasticity and applications to black-filled elastomers*, J. Mech. Phys. Solids, **48**, pp. 1389-1411, (2000)

[5] I. Tremizer, P. Wriggers, *An adaptive method for homogenization in orthotropic nonlinear elasticity*, Comput. Methods in App. Mech. Eng.g, **196**, pp. 3409-3423 (2006)

[6] F. Cirak, M. Ortiz *Fully C^1-conforming subdivision elements for finite deformation thin-shell analysis*, International Journal for Numerical Methods in Engineering, **51**, pp. 757-885 , (2001)

[7] P. Betsch, F. Gruttmann, E. Stein, *A 4-node finite shell element for the implementation of general hyperelastic 3D-elasticity at finite strains*, Comput. Methods in App. Mech. Eng., **130**, pp. 57-79 (1996)

[8] E. W. C. Coenen, V. G. Kouznetsova, M. G. D. Geers, *Computational homogenization for heterogeneous thin sheets*, Int. j. for numer. methods eng., **83**, pp. 1180-1205, (2010)

[9] B. C. N. Mercatoris, T. J. Massart, *A coupled two-scale computational scheme for the failure of periodic quasi-brittle thin planar shells and its application to masonry*, Int. j. for numer. methods eng., **85**, pp. 1177-1206, (2011)

[10] R. Hill *Elastic properties of reinforced solids: Some theoretical principles*, J. Mech. Phys. Solids, **11**, pp. 357-372, (1963)

[11] W.J. Drugan, J.R. Willis, *A micromechanics-based nonlocal constitutive equation and estimates of representative volume element size for elastic composites*, J. Mech. Phys. Solids, **44**, pp. 497-524 (1996)

[12] Zienkiewicz, O.C. and Taylor, R.L. *The finite element method*. McGraw Hill, Vol. I., (1989), Vol. II., (1991).

[13] Idelsohn, S.R. and Oñate, E. Finite element and finite volumes. Two good friends. *Int. J. Num. Meth. Engng.* (1994) **37**:3323–3341.